Acetylene: A Key Growth Precursor for Single-Walled Carbon Nanotube Forests

ARTICLE *in* THE JOURNAL OF PHYSICAL CHEMISTRY C · OCTOBER 2009

Impact Factor: 4.77 · DOI: 10.1021/jp905134b

Acetylene: A Key Growth Precursor for Single-Walled Carbon Nanotube Forests

G. Zhong,*,† S. Hofmann,† F. Yan,† H. Telg,‡ J. H. Warner,§ D. Eder,|| C. Thomsen,‡ W. I. Milne,† and J. Robertson†

Department of Engineering, University of Cambridge, 9 JJ Thomson Avenue, Cambridge CB3 0FA, United Kingdom, Institut für Festkörperphysik, Technische Universität Berlin, Hardenbergstrasse 36, 10623 Berlin, Germany, Department of Materials, University of Oxford, Oxford OX1 3PH, United Kingdom, Department of Materials Science and Metallurgy, University of Cambridge, Cambridge CB2 3QZ, United Kingdom

Received: June 1, 2009; Revised Manuscript Received: July 24, 2009

The growth of tall, single-walled carbon nanotube (SWNT) forests is often believed to require the use of specific feedstocks (e.g., ethanol) or etchants (e.g., water). Here, on the basis of mass spectrometry for hydrogen-diluted methane in a microwave plasma-enhanced chemical vapor deposition (PECVD) reactor, we develop a purely thermal CVD process for SWNT forests *without* an etchant gas. The thermally grown SWNT forests are found to have a similar high quality, purity, growth rate, areal density, diameter, and chirality distribution as in the PECVD case. We show that C_2H_2 is the main growth precursor, and suggest more generally that feedstock conversion to C_2H_2 is of key importance to SWNT forest CVD. A reactive etchant, such as water, atomic hydrogen, or hydroxyl radicals, can widen the SWNT forest deposition window but is not required in cold-wall reactors at low pressures.

Dense, vertically aligned forests of carbon nanotubes (CNTs) are being developed for a wide range of applications, such as interconnects in integrated circuits, thermal management systems, adhesive surfaces, supercapacitor electrodes, and microelectromechanical systems.[1−9] There are many reports on the chemical vapor deposition (CVD) of tall, vertically aligned mats of multi-walled carbon nanotubes (MWNTs).[1,5,10,11] The growth of high-quality, single-walled carbon nanotube (SWNT) mats at high yield is, however, less common[12−17] and remains challenging. This challenge appears 2-fold: (1) to devise an efficient catalyst system for high densities[18−21] and (2) to control the carbon activity at the growth site by using an appropriate feedstock or etchant gas, such as water, to maintain an active catalyst.[22,23]

There is often a desire to lower the SWNT growth temperature; for example, to enhance compatibility with Si process technology. A general approach is to activate precursors with a plasma or hot filament.[24,25] Plasma-enhanced CVD (PECVD) is also reported to give preferential growth of semiconducting nanotubes by some groups.[26,27] Such selective control of SWNT properties by choice of catalyst and process conditions would widen the application potential. However, to date, the role of plasma/hot filament enhancement is still contentious. Overall, some basic questions need clarification: (1) the role of the plasma during growth, (2) the nature of the growth species, (3) the need for and role of an etchant.

We recently employed remote microwave PECVD to grow tall, high-density SWNT mats.[14,19,28] In this letter, we couple this remote microwave PECVD growth reactor to a thermal CVD system equipped with a mass spectrometer. We reproduce the local gas conditions of the remote plasma by a simple gas mixture and then use this to grow essentially identical SWNT mats by cold-wall thermal CVD without a plasma. This allows us to clarify each of the issues above. We find that plasma excitation is not necessary for SWNT forest growth, acetylene is the primary growth species, and a reactive etchant (e.g., water, atomic hydrogen or hydroxyl radicals) is not required in cold-wall reactors if the hydrocarbon activity is low. We thereby develop simple thermal CVD conditions for the scalable growth of high-density SWNT mats. For our CVD conditions and the widely used Fe/Al_2O_3 catalyst system, we find no enrichment of semiconducting or metallic SWNTs.

We use an Astex-style 2.45 GHz microwave plasma system in a stainless steel chamber of base pressure 10^{-5} mbar, as commonly used in diamond CVD. Substrates are heated on a boron nitride-coated graphite (PBN/PG) heater element kept ∼45 mm away from the plasma ball and separated by a plate mesh, which confines the plasma away from the substrate but allows free transport of gaseous species to the substrate. The temperature of the heater element is controlled by a Eurotherm 3216 controller and monitored by a type C thermocouple. The thermocouple feedback balances indirect substrate heating by the plasma, which is small under remote conditions. The gas outflow of the microwave plasma reactor is connected to a second, cold-wall stainless steel CVD chamber with 10^{-8} mbar base pressure (equipped with a similar heater element). A differentially pumped electrostatic quadrupole plasma (EQP) mass spectrum analyzer (Hiden Analytical) is attached to the second chamber.

The substrates are polished Si(100) wafers sputter-coated with nominally 0.5 nm Al (top layer)/0.5−0.7 nm Fe/10 nm Al. The Al layers oxidize in air to give the Al_2O_3 support layers. Fe/Al_2O_3 support interactions restrict the Fe surface mobility, stabilizing small catalyst nanoparticle dimensions at the elevated CVD temperatures and leading to a high nanotube nucleation density.[21] The nanotube samples are characterized by scanning electron microscopy (SEM, LEO 1530 VP FEGSEM), high resolution transmission electron microscopy (HRTEM, FEI

* Corresponding author. Phone: +44(1223)748317. Fax: +44(1223)748348. E-mail: gz222@cam.ac.uk.
† Department of Engineering, University of Cambridge.
‡ Technische Universität Berlin.
§ University of Oxford.
|| Department of Materials Science and Metallurgy, University of Cambridge.

10.1021/jp905134b CCC: $40.75
Published on Web 09/11/2009

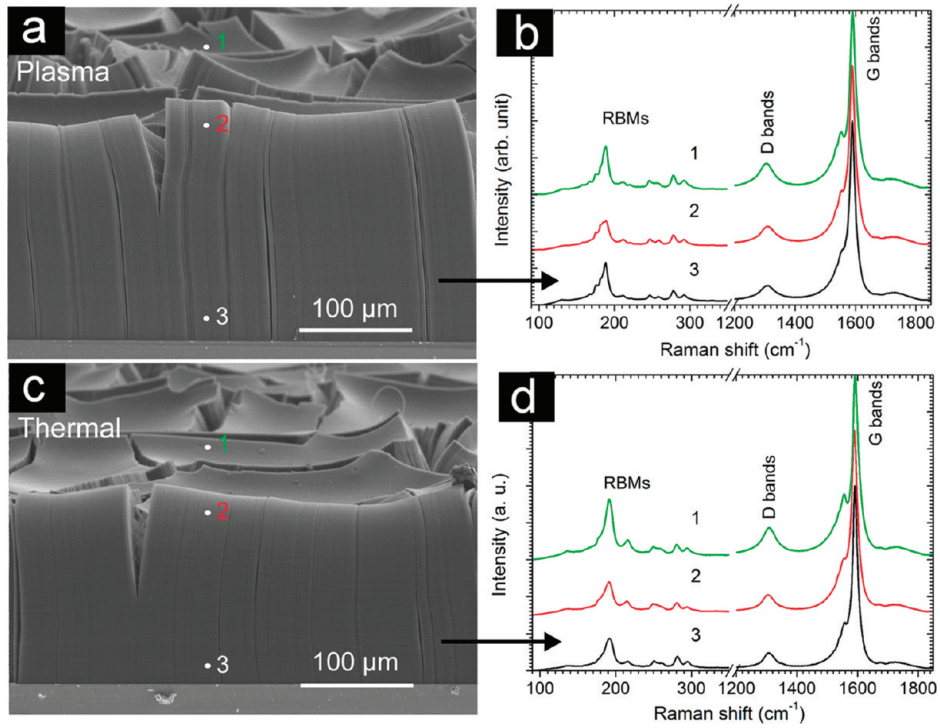

Figure 1. SEM images and Raman spectra of (a, b) SWNT forest grown by remote microwave PECVD in 20:180 sccm CH_4/H_2 for 10 min and of (c, d) SWNT forest grown by thermal CVD in 5:195 sccm C_2H_2/H_2 for 10 min. The total pressure was 15 mbar for both depositions. The labeling indicates the position of the different Raman measurements. The Raman spectra are normalized to the G band intensity; the excitation wavelength is 633 nm.

Titan), Raman spectroscopy (Dilor XY800 spectrometer with triple monochromator, Ar−Kr laser and tunable lasers, and Renishaw 1000), and thermogravimetric analysis (TGA, TA-Q500).

We use the following standard conditions for PECVD:[29] (1) preheat the substrates to 650 °C for 5 min in 20:180 sccm CH_4/H_2 at 15 mbar, (2) ignite the 600 W microwave plasma to start nanotube growth. Figure 1a, b shows a cross-sectional SEM image and Raman spectra of an as-grown SWNT forest. Millimeter-high forests can be achieved,[28] but here, we stopped growth after 10 min to give a 200-μm-high forest, an average growth rate of ~20 μm/min. The large cracks indicate a high SWNT density, which we estimate to be $\sim 10^{12}$ cm^2.[19,29] Note that for hydrogen/methane mixtures, nanotubes grow only when the plasma is *on*. Hence, the growth species is not methane, but a long-lived species created by the plasma, such as the methyl monoradical or the acetylene molecule.

Figure 2a shows the EQP mass spectrum of neutral species probed downstream of the microwave chamber under the growth conditions of Figure 1a. The second CVD reactor and the EQP probe were thereby differentially pumped to 0.4 mbar and 1.1×10^{-6} mbar, respectively. The mass spectra are simpler than those found when directly probing in a CH_4/H_2 plasma.[30] For the two-chamber setup, we probe only relatively stable species. At 15 mbar, the mean free path of gas species is a few micrometers, so short-lived diradicals and ions such as C and CH_2 do not contribute. Apart from the CH_4 feed gas, Figure 2a shows C_2H_2 (26, 25 amu) and C_2H_4 (28, 27, 26, 25 amu). Other hydrocarbon species over 80 amu are negligible. Note that *m*/*z* assignments can be ambiguous, with, for example, *m*/*z* 28 amu in the baseline mass spectrum corresponding to either N_2 or CO. However, the conversion yield of CH_4 to C_2H_2 and C_2H_4 varies with plasma power, allowing a clear assignment of these peaks.

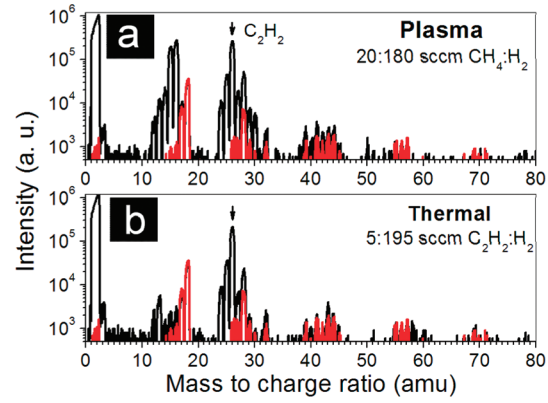

Figure 2. Mass spectrum of neutral species from (a) microwave plasma in 20:180 sccm CH_4/H_2 (600 W power) compared to (b) thermal CVD atmosphere of 5:195 sccm C_2H_2/H_2. The reactor pressure was 15 mbar in both cases. The plasma atmosphere was sampled downstream. The main peak of the C_2H_2 fragmentation pattern is indicated. The residual mass spectra at $\sim 10^{-7}$ mbar base pressure are shown in red.

To unambiguously identify the growth species, we reproduced the main features of the mass spectrum for the 20:180 sccm CH_4/H_2 microwave plasma in Figure 2a by a 9.6:4.4:185 sccm $CH_4/C_2H_2/H_2$ gas mixture *without* plasma. Because C_2H_2 is the dominant reactive species for plasma excitation at 15 mbar[24,30] and because CH_4 does not contribute to SWNT growth, we simplified this to a 5:195 sccm C_2H_2/H_2 mixture for thermal growth. Figure 2b shows the resulting mass spectrum for the same total pressures as the plasma conditions above. Note that commercial C_2H_2 gas cylinders contain acetone, giving a low purity of ~99.6%. The 43 amu in Figure 2b corresponds to acetone. However, this subtle difference does not affect SWNT forest growth. Acetone is a weak precursor for SWNT CVD,[31] and we note that acetone contains oxygen, hence it might act as growth enhancer similar to H_2O. We emphasize that our

remote PECVD growth atmosphere has no acetone contamination, but nevertheless gives the same SWNT mats.

Our thermal CVD process is as follows: (1) the samples are heated to 650−700 °C for 5 min under 200 sccm H_2 at 15 mbar, and (2) C_2H_2 is added and a flow rate of 5:195 sccm C_2H_2/H_2 is established for nanotube growth. Figure 1c shows a typical SWNT forest grown under these cold-wall thermal CVD conditions. The growth rate, SEM topography, and Raman signature are very similar to those from the microwave PECVD in Figure 1a, b. The successful thermal growth from C_2H_2/H_2 in a cold-wall reactor confirms that C_2H_2 is the main growth species of SWNT forests in both plasma-assisted and thermal CVD. This is consistent with the molecular beam data of Eres et al.[31] In addition, Sugime et al.[32] has shown that C_2H_2 is among the decomposition products of C_2H_5OH for hot-wall furnace conditions. Hence, in general, we suggest that acetylene is the key precursor for a large range of CVD processes leading to CNT forest growth, including alcohol or ethylene in hot-wall CVD reactors. In addition, there is no etchant in our process conditions because atomic hydrogen is not produced at 650 °C.

Extending our growth time for thermal CVD from 10 min to 1.5 h produces 1.4-mm-high SWNT forests. The SWNT length increases almost linearly with time, and SWNT quality remains almost unchanged.[28,29] In contrast, atmospheric pressure hot-wall CVD exhibits fast SWNT growth, terminating abruptly after some tens of minutes, whereas longer growth times give codeposition of carbonaceous overlayers.[22,33] Hot-wall conditions can cause hydrocarbon cracking and polymerization in the gas phase. Hence, similar to plasma/hot filament conditions, we suggest that etchants are of high importance to minimize amorphous carbon deposition and to yield high-quality SWNT forests.[16,23,34] On the other hand, in our cold-wall reactor, etchants appear to have little effect on SWNT growth so that a carefully calibrated thermal CVD atmosphere can replace the balance between active carbon and etchant species in hot-wall CVD or plasma/hot filament conditions. The growth-prolonging etching effects of water, oxygen, or atomic hydrogen are more critical for hot-wall systems. Another factor is that a high carbon activity, such as a high hydrocarbon partial pressure, can lead to MWNT growth instead of SWNTs. This is because if the carbon supply is too fast, more walls grow.[35]

To investigate the effects of water in our cold-wall CVD, we intentionally introduced up to 20 sccm H_2O via a needle-valve-controlled inlet into the second CVD chamber, together (via a separate inlet) with the outflow of the 20:180 sccm CH_4/H_2 (600 W power) microwave plasma from the first chamber at 15 mbar, then switched on the PBN/PG heater to start nanotube growth. This H_2O level is very high compared to the ~100 ppm levels used by Futaba et al.[22] Figure 3a shows the mass spectrum. Compared to Figure 2a, the H_2O peak at 18 amu is clearly increased. Even at such high water levels, nanotube forests nucleate (Figure 3b). H_2O variations from 0 to 20 sccm showed no acceleration or prolongation of the forest growth. In fact, the forest in Figure 3b mainly consists of MWNTs, which we attribute to the different pretreatment; in particular, to heating up in a C_2H_2-containing atmosphere. Here, water appears to also not have affected the coarsening of the Fe catalyst film.[36] Water in our cold-wall CVD conditions does not act as an efficient etchant, but neither is it needed.

A further series of experiments allowed us to identify C_2H_2 injection/concentration and catalyst pretreatment as key parameters for SWNT forest nucleation. Under otherwise identical conditions at a total flow rate of 200 sccm, the nanotube growth rate increases for C_2H_2 concentrations from 1% to 10% and

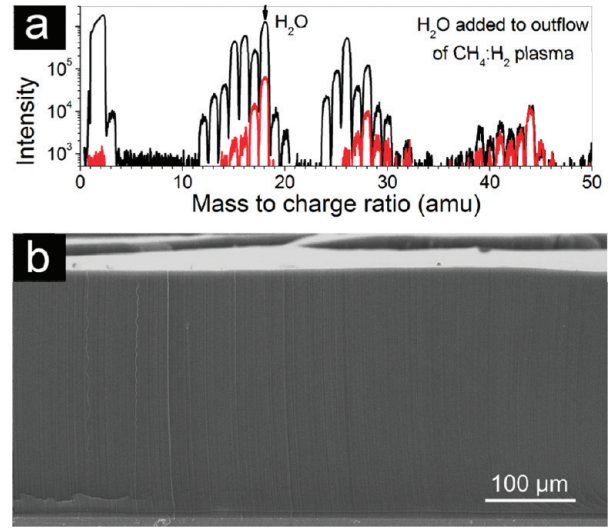

Figure 3. The effect of water on CNT growth in a cold-wall CVD system: (a) Mass spectrum of CVD atmosphere created by adding 20 sccm H_2O to the outflow of the 20:180 sccm CH_4/H_2 (600 W power) microwave plasma. The background mass spectrum at ~10^{-7} mbar is plotted in red. (b) SEM images of the CNT forest grown in this CVD atmosphere at 15 mbar in 10 min.

then falls with a further increase to 15%. Raman measurements show, however, that for 5−7.5% C_2H_2, the samples are mixtures of SWNTs and MWNTs with stronger D peaks and weaker radial breathing mode (RBM) signatures. At over 10% C_2H_2, the nanotubes are mainly MWNTs with no RBM modes and a D/G ratio close to 1. The transition from SWNTs to MWNTs is in agreement with the nanotube growth model of Wood et al.,[35] which, however, does not correctly reflect our growth rate changes.

The Raman spectra of the CVD and PECVD nanotubes show sharp RBMs at 100−350 cm^{-1}, a two-peaked G band at 1590 $cm^{-1,}$ and a low-intensity D band (1330 cm^{-1}), indicative of high-quality SWNTs. Raman spectra (Figure 1d) measured at the forest surface and various cross-sectional positions show little variation, suggesting sample homogeneity. Figure 4a shows a detailed comparison of RBM spectra measured at multiple wavelengths, which allows chiral indexing and distinguishes between metallic (M) and semiconducting (S) SWNTs.[7] The chiral distribution map of Figure 4b shows that the SWNT forests grown by microwave PECVD and thermal CVD have a similar broad diameter distribution. All tube chiralities ($0° \leq \theta \leq 30°$) are present, with no enrichment of semiconducting SWNTs. There is an interesting contrast to Qu et al.[27] and Li et al.,[26] who report preferential growth of semiconducting SWNTs from similar catalyst films by low pressure C_2H_2 and Ar-diluted CH_4 PECVD, respectively.

The HRTEM images in Figure 5 indicate that our SWNT forests are of very high purity and quality. There were not only no signs of any Fe catalysts or obvious amorphous carbon but also no MWNTs or double-walled nanotubes (DWNTs). Direct imaging of the atomic structure enabled the SWNT chiralities to be assigned. Figure 5a(i) shows a small, 0.9-nm-diameter SWNT that is indexed as (10, 3). Figure 5a(ii) shows a larger, 2.59-nm-diameter SWNT, which is indexed as (23, 15). The nanotube diameters were measured by taking a line profile perpendicular to the tube axis, and the chiral angle vector for (n, m) assignment was measured from the optical diffraction produced in the 2D fast Fourier transform. The diameters for ~40 tubes have a broad distribution over 0.5−3 nm, with an average of 1.3 nm (Figure 5b). This is consistent with the Raman

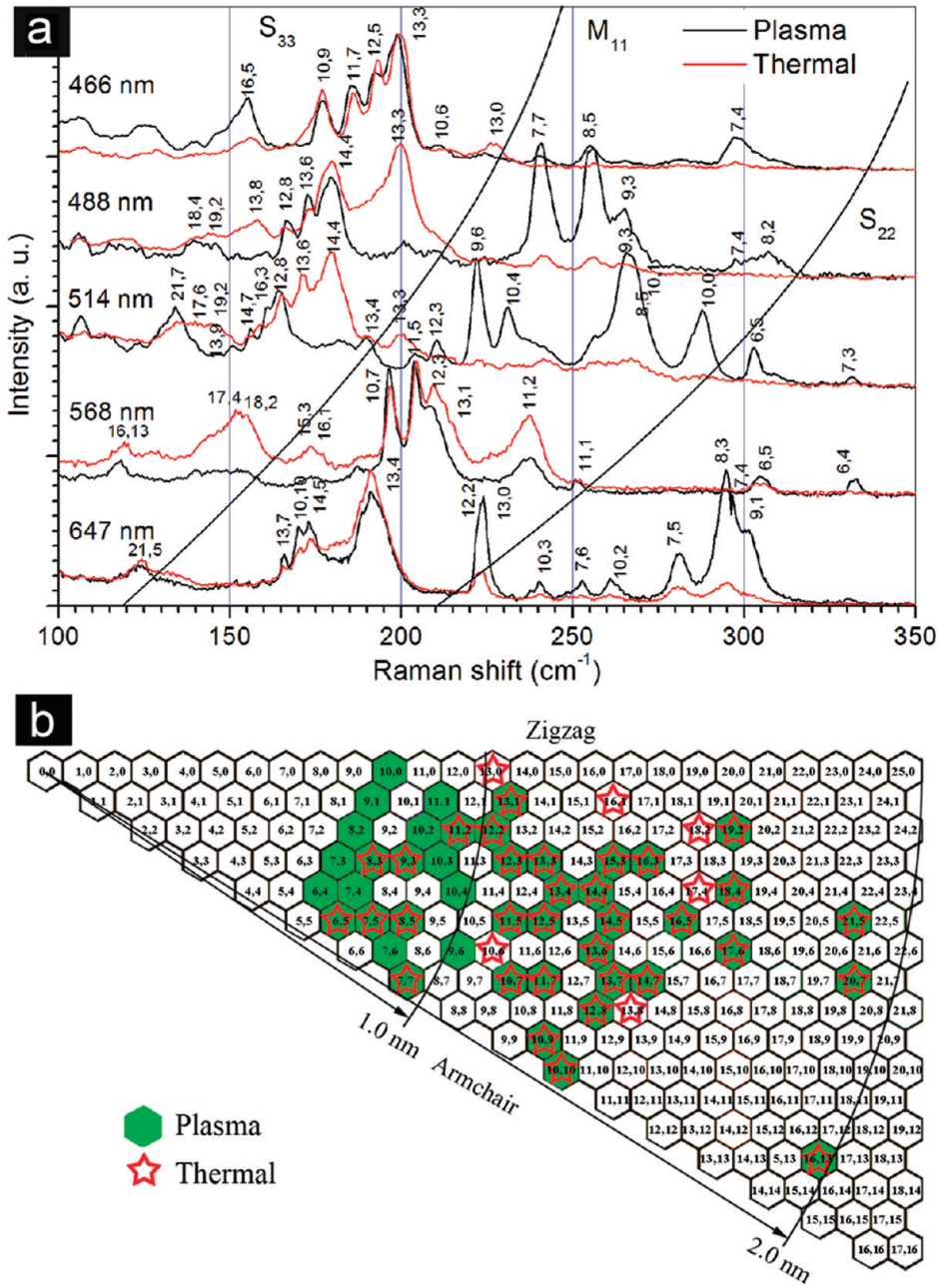

Figure 4. (a) Raman radial breathing modes excited at multiple laser wavelengths for SWNT forests grown by microwave PECVD in 20:180 sccm CH_4/H_2 (600 W power) and by thermal CVD in 5:195 sccm C_2H_2/H_2. The spectral range is divided into zones corresponding to modes of metallic (M11) and semiconducting (S22, S33) tubes. (b) Chirality distribution map of the two samples based on assignments in panel a. Lines of constant tube diameters (1.0 and 2.0 nm) are indicated.

analysis of Figure 4b. The broad diameter and chirality distributions are similar to those from hot-wall, water-assisted CVD,[37] but because we use a thinner catalyst layer, the mean diameter is lower in the 0.5−3.0 nm range.

The nanotube quality was further checked by TGA. We find the oxidation temperatures of SWNT forests grown by thermal CVD and PECVD to be similar. The derivative spectrum shows one sharp peak at ~675 °C, corresponding to SWNT combustion from 550 to 750 °C. The thermal CVD samples show lower amorphous carbon content, agreeing with the HRTEM data.

We previously showed that a narrow Fe thickness range (0.3−0.7 nm) on Al_2O_3 support, followed by a short 5 min thermal pretreatment in reducing conditions of H_2 or CH_4/H_2 leads to PECVD growth of high-density (10^{12} cm^2) SWNT forests.[19] We find the same for our thermal CVD conditions. In-situ XPS studies identified metallic Fe as the active growth catalyst.[38] The interaction between Fe and Al_2O_3 does enhance forest nucleation.[21] The initially oxidized Fe film must first be reduced. However, once reduced, the Fe nanoparticles are prone to coarsening. Catalyst films thicker than 1 nm or a heat pretreatment longer than 20 min would inevitably result in nucleation and growth of DWNTs/MWNTs due to the formation of large catalyst particles. It was recently reported that increases in the nanotube areal density can be achieved by the delayed introduction of H_2.[39] We emphasize that our thermally grown SWNT forests have an areal density that is about 2 orders of magnitude higher than reported for those MWNT forests.

Summarizing, by analyzing the gas composition of a remote plasma reactor, we have been able to develop a thermal CVD process to grow high-purity, high-density SWNT forests without

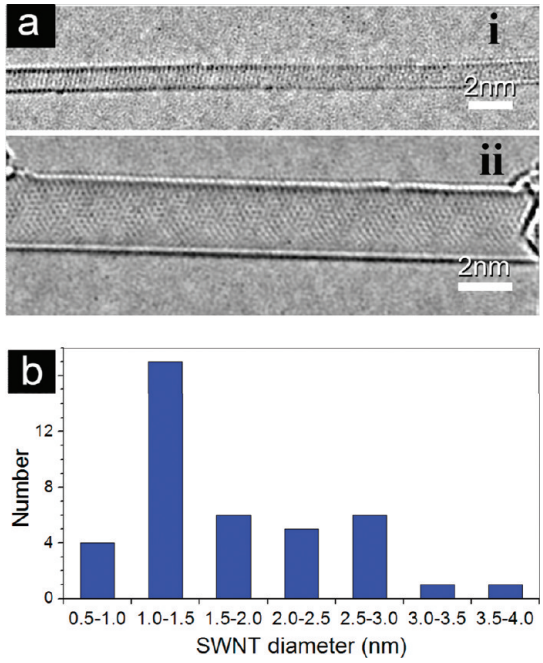

Figure 5. (a) HRTEM images of (i) a 0.9-nm-diameter SWNT indexed to (10, 3) chirality and (ii) a 2.59-nm-diameter SWNT assigned to a (23, 15) chirality, grown by thermal CVD in 5:195 sccm C_2H_2/H_2 for 10 min. (b) SWNT diameter distribution from analysis of sample shown in panel a.

the presence of an etchant gas. The process is possible using a cold-wall reactor, which reduces hydrocarbon pyrolysis and polymerization reactions, which reduces the need for an etchant. We showed that acetylene is the growth precursor, and the ignition of a plasma acts as a fast gas switch converting CH_4 to C_2H_2. This suggests remote plasma-assisted CVD could be replaced by thermal cold-wall CVD for larger-scale production of SWNT forests.

Acknowledgment. Support by the European Community (VIACARBON) is gratefully acknowledged. This work was also supported in part by EPSRC, ESF and the EC Sixth Framework Programme under Contract No. ERAS-CT-2003-980409. J.R. thanks the Humboldt Foundation for support in Berlin. S.H. acknowledges funding from the Royal Society and Peterhouse, Cambridge. J.H.W. thanks the support from the Glasstone Fund and Brasenose College, Oxford. D.E. acknowledges the Austrian Academy of Science (APART Program) for financial support.

References and Notes

(1) Fan, S. S.; Chapline, M. G.; Franklin, N. R.; Tombler, T. W.; Cassell, A. M.; Dai, H. J. *Science* **1999**, *283*, 512–514.
(2) Ngo, Q.; Cruden, B. A.; Cassell, A. M.; Sims, G.; Meyyappan, M.; Li, J.; Yang, C. Y. *Nano Lett.* **2004**, *4*, 2403–2407.
(3) Futaba, D. N.; Hata, K.; Yamada, T.; Hiraoka, T.; Hayamizu, Y.; Kakudate, Y.; Tanaike, O.; Hatori, H.; Yumura, M.; Iijima, S. *Nat. Mater.* **2006**, *5*, 987–994.
(4) Huang, H.; Liu, C. H.; Wu, Y.; Fan, S. S. *Adv. Mater.* **2005**, *17*, 1652–1656.
(5) Li, X. S.; Cao, A. Y.; Jung, Y. J.; Vajtai, R.; Ajayan, P. M. *Nano Lett.* **2005**, *5*, 1997–2000.
(6) Nihei, M.; Kawabata, A.; Awano, Y. *Jpn. J. Appl. Phys., Part 2* **2003**, *42*, L721–L723.
(7) Robertson, J.; Zhong, G.; Telg, H.; Thomsen, C.; Warner, J. H.; Briggs, G. A. D.; Dettlaff-Weglikowska, U.; Roth, S. *Appl. Phys. Lett.* **2008**, *93*, 163111.
(8) Qu, L. T.; Dai, L. M.; Stone, M.; Xia, Z. H.; Wang, Z. L. *Science* **2008**, *322*, 238–242.
(9) Hayamizu, Y.; Yamada, T.; Mizuno, K.; Davis, R. C.; Futaba, D. N.; Yumura, M.; Hata, K. *Nat. Nanotechnol.* **2008**, *3*, 289–294.
(10) Eres, G.; Puretzky, A. A.; Geohegan, D. B.; Cui, H. *Appl. Phys. Lett.* **2004**, *84*, 1759–1761.
(11) Hart, A. J.; Slocum, A. H. *J. Phys. Chem. B* **2006**, *110*, 8250–8257.
(12) Pinault, M.; Pichot, V.; Khodja, H.; Launois, P.; Reynaud, C.; Mayne-L'Hermite, M. *Nano Lett.* **2005**, *5*, 2394–2398.
(13) Hata, K.; Futaba, D. N.; Mizuno, K.; Namai, T.; Yumura, M.; Iijima, S. *Science* **2004**, *306*, 1362–1364.
(14) Zhong, G. F.; Iwasaki, T.; Honda, K.; Furukawa, Y.; Ohdomari, I.; Kawarada, H. *Jpn. J. Appl. Phys., Part 1* **2005**, *44*, 1558–1561.
(15) Zhang, L.; Tan, Y. Q.; Resasco, D. E. *Chem. Phys. Lett.* **2006**, *422*, 198–203.
(16) Xu, Y. Q.; Flor, E.; Schmidt, H.; Smalley, R. E.; Hauge, R. H. *Appl. Phys. Lett.* **2006**, *89*, 123116.
(17) Murakami, Y.; Chiashi, S.; Miyauchi, Y.; Hu, M. H.; Ogura, M.; Okubo, T.; Maruyama, S. *Chem. Phys. Lett.* **2004**, *385*, 298–303.
(18) Futaba, D. N.; Hata, K.; Namai, T.; Yamada, T.; Mizuno, K.; Hayamizu, Y.; Yumura, M.; Iijima, S. *J. Phys. Chem. B* **2006**, *110*, 8035–8038.
(19) Zhong, G. F.; Iwasaki, T.; Kawarada, H. *Carbon* **2006**, *44*, 2009–2014.
(20) Kondo, D.; Sato, S.; Awano, Y. *Chem. Phys. Lett.* **2006**, *422*, 481–487.
(21) Mattevi, C.; Wirth, C. T.; Hofmann, S.; Blume, R.; Cantoro, M.; Ducati, C.; Cepek, C.; Knop-Gericke, A.; Milne, S.; Castellarin-Cudia, C.; Dolafi, S.; Goldoni, A.; Schloegl, R.; Robertson, J. *J. Phys. Chem. C* **2008**, *112*, 12207–12213.
(22) Futaba, D. N.; Hata, K.; Yamada, T.; Mizuno, K.; Yumura, M.; Iijima, S. *Phys. Rev. Lett.* **2005**, *95*, 056104.
(23) Yamada, T.; Maigne, A.; Yudasaka, M.; Mizuno, K.; Futaba, D. N.; Yumura, M.; Iijima, S.; Hata, K. *Nano Lett.* **2008**, *8*, 4288–4292.
(24) Meyyappan, M.; Delzeit, L.; Cassell, A.; Hash, D. *Plasma Sources Sci. Technol.* **2003**, *12*, 205–216.
(25) Dillon, A. C.; Mahan, A. H.; Parilla, P. A.; Alleman, J. L.; Heben, M. J.; Jones, K. M.; Gilbert, K. E. H. *Nano Lett.* **2003**, *3*, 1425–1429.
(26) Li, Y. M.; Mann, D.; Rolandi, M.; Kim, W.; Ural, A.; Hung, S.; Javey, A.; Cao, J.; Wang, D. W.; Yenilmez, E.; Wang, Q.; Gibbons, J. F.; Nishi, Y.; Dai, H. J. *Nano Lett.* **2004**, *4*, 317–321.
(27) Qu, L. T.; Du, F.; Dai, L. M. *Nano Lett.* **2008**, *8*, 2682–2687.
(28) Zhong, G. F.; Iwasaki, T.; Robertson, J.; Kawarada, H. *J. Phys. Chem. B* **2007**, *111*, 1907–1910.
(29) Zhong, G. F.; Iwasaki, T.; Honda, K.; Furukawa, Y.; Ohdomari, I.; Kawarada, H. *Chem. Vap. Deposition* **2005**, *11*, 127–130.
(30) Fujii, T.; Kareev, M. *J. Phys. Chem. A* **2001**, *105*, 4923–4927.
(31) Eres, G.; Kinkhabwala, A. A.; Cui, H. T.; Geohegan, D. B.; Puretzky, A. A.; Lowndes, D. H. *J. Phys. Chem. B* **2005**, *109*, 16684–16694.
(32) Sugime, H.; Noda, S.; Maruyama, S.; Yamaguchi, Y. *Carbon* **2009**, *47*, 234–241.
(33) Yasuda, S.; Hiraoka, T.; Futaba, D. N.; Yamada, T.; Yumura, M.; Hata, K. *Nano Lett.* **2009**, *9*, 769–773.
(34) Zhang, G. Y.; Mann, D.; Zhang, L.; Javey, A.; Li, Y. M.; Yenilmez, E.; Wang, Q.; McVittie, J. P.; Nishi, Y.; Gibbons, J.; Dai, H. J. *Proc. Natl. Acad. Sci. U.S.A.* **2005**, *102*, 16141–16145.
(35) Wood, R. F.; Pannala, S.; Wells, J. C.; Puretzky, A. A.; Geohegan, D. B. *Phys. Rev. B* **2007**, *75*, 235446.
(36) Amama, P. B.; Pint, C. L.; McJilton, L.; Kim, S. M.; Stach, E. A.; Murray, P. T.; Hauge, R. H.; Maruyama, B. *Nano Lett.* **2008**, *9*, 44–49.
(37) Yamada, T.; Namai, T.; Hata, K.; Futaba, D. N.; Mizuno, K.; Fan, J.; Yudasaka, M.; Yumura, M.; Iijima, S. *Nat. Nano* **2006**, *1*, 131–136.
(38) Hofmann, S.; Blume, R.; Wirth, C. T.; Cantoro, M.; Sharma, R.; Ducati, C.; Havecker, M.; Zafeiratos, S.; Schnoerch, P.; Oestereich, A.; Teschner, D.; Albrecht, M.; Knop-Gericke, A.; Schlogl, R.; Robertson, J. *J. Phys. Chem. C* **2009**, *113*, 1648–1656.
(39) Nessim, G. D.; Hart, A. J.; Kim, J. S.; Acquaviva, D.; Oh, J.; Morgan, C. D.; Seita, M.; Leib, J. S.; Thompson, C. V. *Nano Lett.* **2008**, *8*, 3587–3593.

JP905134B